

CREEP BEHAVIOR OF GFRP LAMINATES AND THEIR PHASES: EXPERIMENTAL INVESTIGATION AND ANALYTICAL MODELING

Valentino Paolo Berardi^a, Michele Perrella^b, Luciano Feo^a, Gabriele Cricri^b

^a*Department of Civil Engineering, University of Salerno, Via Giovanni Paolo II 132, Fisciano (SA), Italy*

^b*Department of Industrial Engineering, University of Salerno, Via Giovanni Paolo II 132, Fisciano (SA), Italy*

ABSTRACT

Fibre reinforced polymer (FRP) laminates are being currently used within industrial, automotive, naval, aerospace and civil fields. The reliability of composites over time can be evaluated by characterising their deferred behavior. Experimental investigations on this topic are limited due to the complexity in accurate testing. A creep test program was carried out in order to model the viscous behavior of the composites and their phases. Long term behavior of several unidirectional glass fibre reinforced polymer laminates, manufactured through the wet lay-up technique, and their constituent phases (matrix and fibre) is presented in this paper. Starting from the experimental data acquired for six months, a predictive micromechanical model was proposed for the laminates and the fibres, whilst a phenomenological non linear model, formulated by the authors, was used for the resin matrix. The tests were performed at the Structural Engineering Testing Hall of the University of Salerno.

Keywords: epoxy resin; glass fibres; FRP; long term behavior; creep test; analytical modeling; durability, dimensional stability.

1. INTRODUCTION

Fibre reinforced polymer composites are widely utilized in several fields of engineering as alternative to traditional materials, due to the well-known advantages mainly related to rapid/easy manufacturing, low weight, mouldability, high quality surface finishes and optimal mechanical properties.

In the field of Civil Engineering, composites are mainly adopted in the rehabilitation of existing structures (reinforced concrete and masonry structures), as well as, more recently, in new structures in different shapes (e.g. bars, pultruded elements) [1-5]; in the field of Mechanical Engineering composites are typically used for the manufacturing of industrial, automotive, naval and aerospace structural elements (e.g. machine components, windmill blades, panels) [6-7]; in superconducting systems where insulating composite wraps are bonded to superconducting cables subjected to Lorentz forces [8].

While the short term mechanical behavior of FRPs and strengthening FRP systems was investigated by several researches within many theoretical and experimental studies [1-5], only limited studies were performed on the long term mechanical behavior of these materials and reinforcement systems [9-19]. The viscosity of materials has an important role in design/verification processes, because it can compromise the reliability and durability of these elements [20-27].

In the case of reinforcement of existing structural elements with FRP, the different rheological properties of the components of the strengthened structure (e.g. reinforced concrete core and composite) can lead to a migration of FRP stresses towards the original structural element, compromising the efficacy of the strengthening technique [28-30]. This phenomenon is taken into account in international guide lines on the use of FRP in rehabilitation interventions by means of a simplified and conservative approach, based on a forced limitation of the maximum value of FRP stress at Serviceability Limit State and without considering the rheological properties of the material.

With reference to industrial, automotive, naval and aerospace structural applications, deferred strains of FRPs could not provide appropriate dimensional stability requirements.

In this context, a creep test program on GFRP laminates, manufactured through the wet lay-up technique, and their phases was carried out by the authors at Structural Engineering Testing Hall of Civil Engineering Department of University of Salerno under constant environmental conditions.

The long term behavior of the tested specimens was characterised by using the Burger model and the non linear relationship proposed by the authors [31], starting from experimental strain records of the creep tests.

2. EXPERIMENTAL SET-UP AND SAMPLES

Creep tests on unidirectional GFRP laminates and their phases (epoxy resin and woven unidirectional E-glass tape) were carried out for different stress values at the Structural Engineering Testing Hall of the University of Salerno.

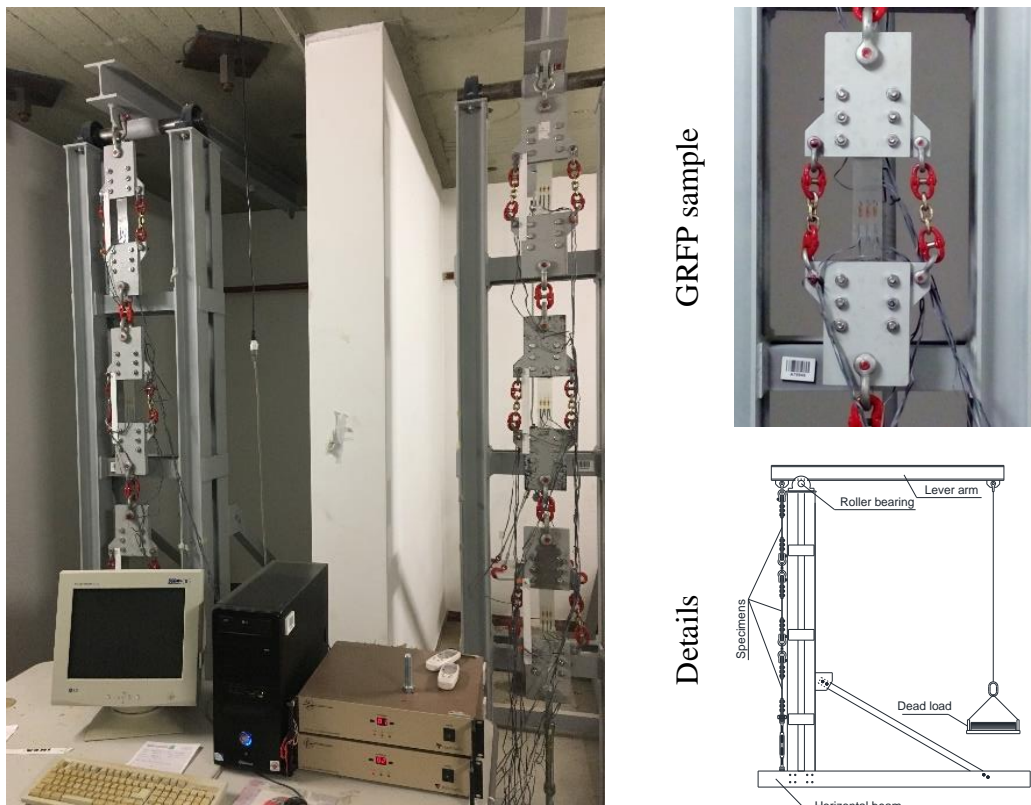


Figure 1. Experimental set-up for the GFRP samples

The experimental program was performed by using three test systems proposed by the authors in previous works [11-12] and upgraded within the present study, capable of applying constant dead loads over time, and two data acquisition systems.

Two steel devices based on an amplification of the dead load through a lever arm were used for the tests on GFRP laminates (Figure 1). A steel frame was utilized to test the fibre and resin samples (Figure 2).

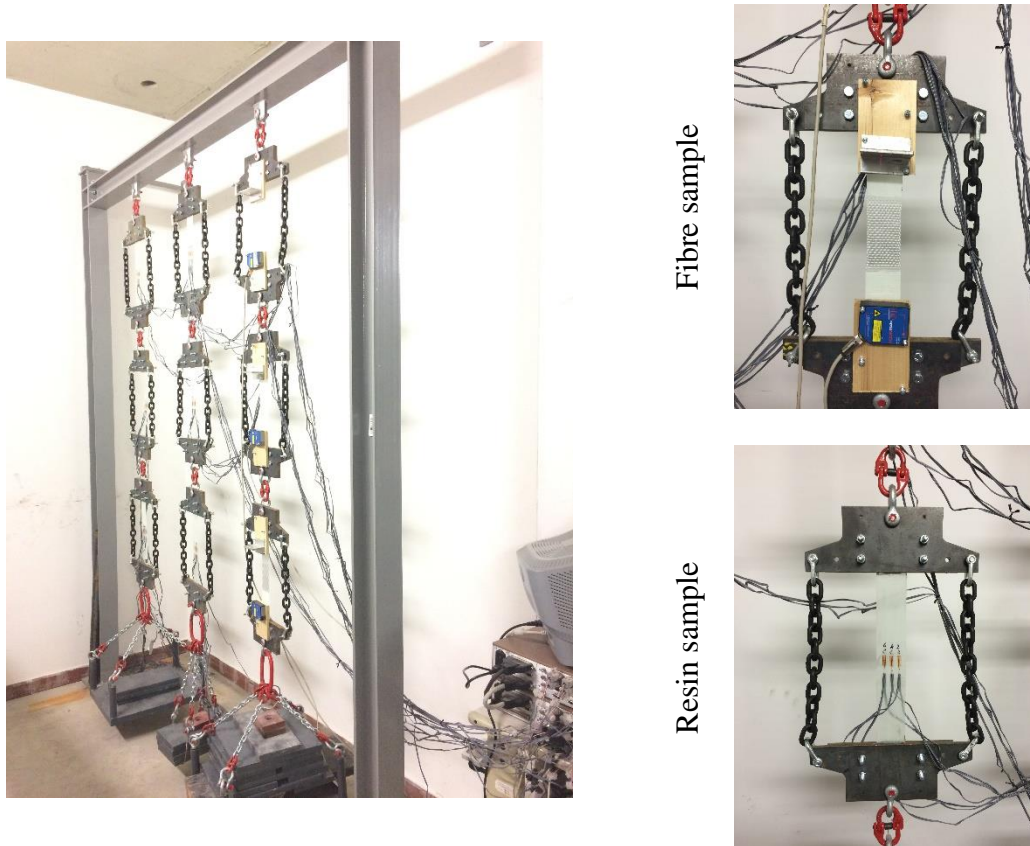


Figure 2. Experimental set-up for the fibre and resin samples

The short time mechanical properties of the unidirectional GFRP laminates, the epoxy resin specimens and the E-glass fibre samples were characterized at the Design Machine Laboratory of the University of Salerno, by performing experimental tests according to ASTM D3039 standard on four specimens for each materials.

The average value of these experimental properties are reported in Tables 1, 2 and 3, where: E_{FRP} and E_f are the longitudinal Young's modulus of the GFRP laminates and of the E-glass fibre samples, respectively; E_m is the Young's modulus of the epoxy resin specimens; f_{FRP} and f_f are the average longitudinal tensile strength of the GFRP laminates and of the E-glass fibre samples (referred to the nominal thickness of 0.42 mm, according to ISO 5084), respectively; f_m is the average tensile strength of the epoxy resin specimens; ν_{FRP} and ν_{mu} are the major Poisson's ratio of the GFRP laminates and of the epoxy resin specimens, respectively; V_f is the volumetric fraction of fibres.

Table 1. GFRP laminate mechanical properties

E_{FRP} [GPa]	f_{FRP} [MPa]	ν_{FRP}	V_f [%]
30.50	650	0.30	50

Table 2. E-glass fibre mechanical properties along longitudinal direction

E_f [GPa]	f_f [MPa]
60.00	1070

Table 3. Epoxy resin mechanical properties

E_m [GPa]	f_m [MPa]	ν_{mu}
3.85	60	0.34

The geometry of the specimens used in the creep test program is depicted in Figure 3.

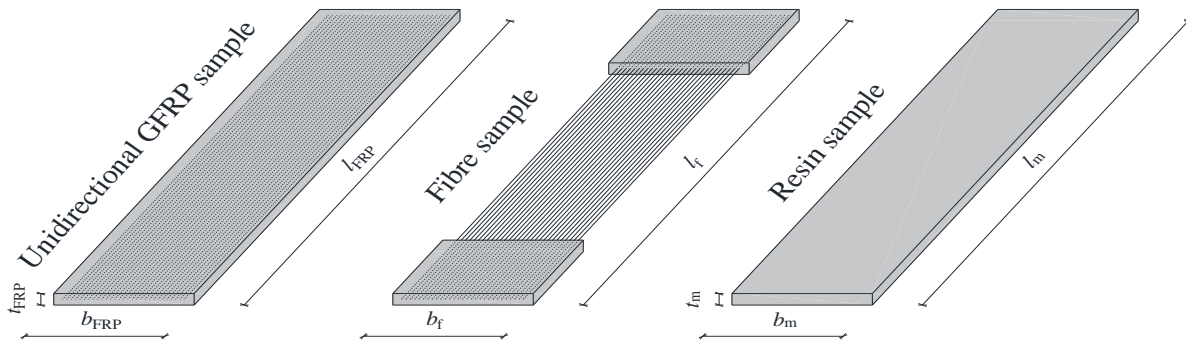


Figure 3. Specimens geometry

The geometrical dimensions of the samples, as well as the area of the GFRP laminates, A_{FRP} , of the E-glass fibre samples, A_f , and of the epoxy resin specimens, A_m , are reported in Tables 4, 5 and 6, being t_f the nominal thickness of fibres. The specimens were cured for 14 days at room temperature.

Table 4. Geometrical properties of the GFRP laminate samples

b_{FRP} [mm]	t_{FRP} [mm]	l_{FRP} [mm]	A_{FRP} [mm ²]
50.0	0.8	410.0	40.0

Table 5. Geometrical and physical properties of the E-glass fibre samples

Number of threads	Linear density of roving [tex]	b_f [mm]	t_f [mm]	l_f [mm]	A_f [mm ²]
60	300	50.0	0.42	410.0	21.0

Table 6. Geometrical properties of the epoxy resin samples

b_m [mm]	t_m [mm]	l_m [mm]	A_m [mm ²]
50.0	0.8	410.0	40.0

The axial force values, N , applied to the sets of samples, the stress values of each sample, σ , and the subsequent tensile strength, f , (corresponding to f_{FRP} in the case of GFRPs, f_f in the case of fibres, f_m in the case of resins) are reported Tables 7, 8 and 9.

Table 7. Experimental stress values in the GFRP specimens

Sample ID	L1	L2	L3	L4	L5	L6
N [N]	3170	3252	3302	6751	6817	6883
σ [MPa]	79.25	81.30	82.56	168.78	170.43	172.08
σ/f_{FRP} [%]	12.19	12.51	12.70	25.97	26.22	26.47

Table 8. Experimental stress values in the glass fibre specimens

Sample ID	F1	F2	F3
N [N]	2772	2804	2854
σ [MPa]	132.01	133.50	135.90
σ/f_k [%]	12.34	12.48	12.70

Table 9. Experimental stress values in the resin specimens

Sample ID	M1	M2	M3	M4	M5	M6
N [N]	433	499	565	651	733	783
σ [MPa]	10.83	12.48	14.13	16.27	18.32	19.58
σ/f_m [%]	18.05	20.80	23.56	27.12	30.53	32.63

The data acquisition system consists of:

- strain gages applied to the GFRP and epoxy resins samples;
- laser probes used for monitoring fibre samples;
- modular scanners and relative data management software, installed on two computers;
- thermocouples.

The adopted scanners was capable of carrying corrections of the data acquisition, due to either the loss of the signal or the instantaneous temperature.

Each fibre sample was equipped with a laser distance meter; each resin and laminate sample with six strain gages symmetrically set out to the middle plane (three strain gages on every single face close to the midspan orientated along the load application axis) in order to compensate for any eventual measuring errors caused by bending deformation.

3. RESULTS OF EXPERIMENTAL TESTS

The experimental data were acquired with a rate of 12 samples per hours during the initial stage of test (about 700 h), for a best evaluation of primary creep phenomenon, whilst successively with a rate of 6 samples per hours.

Let denote L_{i-chj} ($i, j=1, \dots, 6$) the curve corresponding to the j -th strain gage of the i -th laminate specimen; L_i the curve corresponding to the average value of the strain gages data referred to the i -th laminate specimen; F_i ($i=1, \dots, 3$) the curve corresponding to the i -th fibre specimen; M_{i-chj} ($i, j=1, \dots, 6$) the curve corresponding to the j -th strain gage channel of the i -th resin specimen; M_i the curve corresponding to the average value of the strain gages data referred to the i -th resin specimen.

The total strain-time curves of the laminates, fibres and the resins are presented in Figures 4, 5 and 6.

The sets of strain gauges shown in the Figures 4 and 6, have been selected, for each specimen, by excluding the two channels with the higher dispersion.

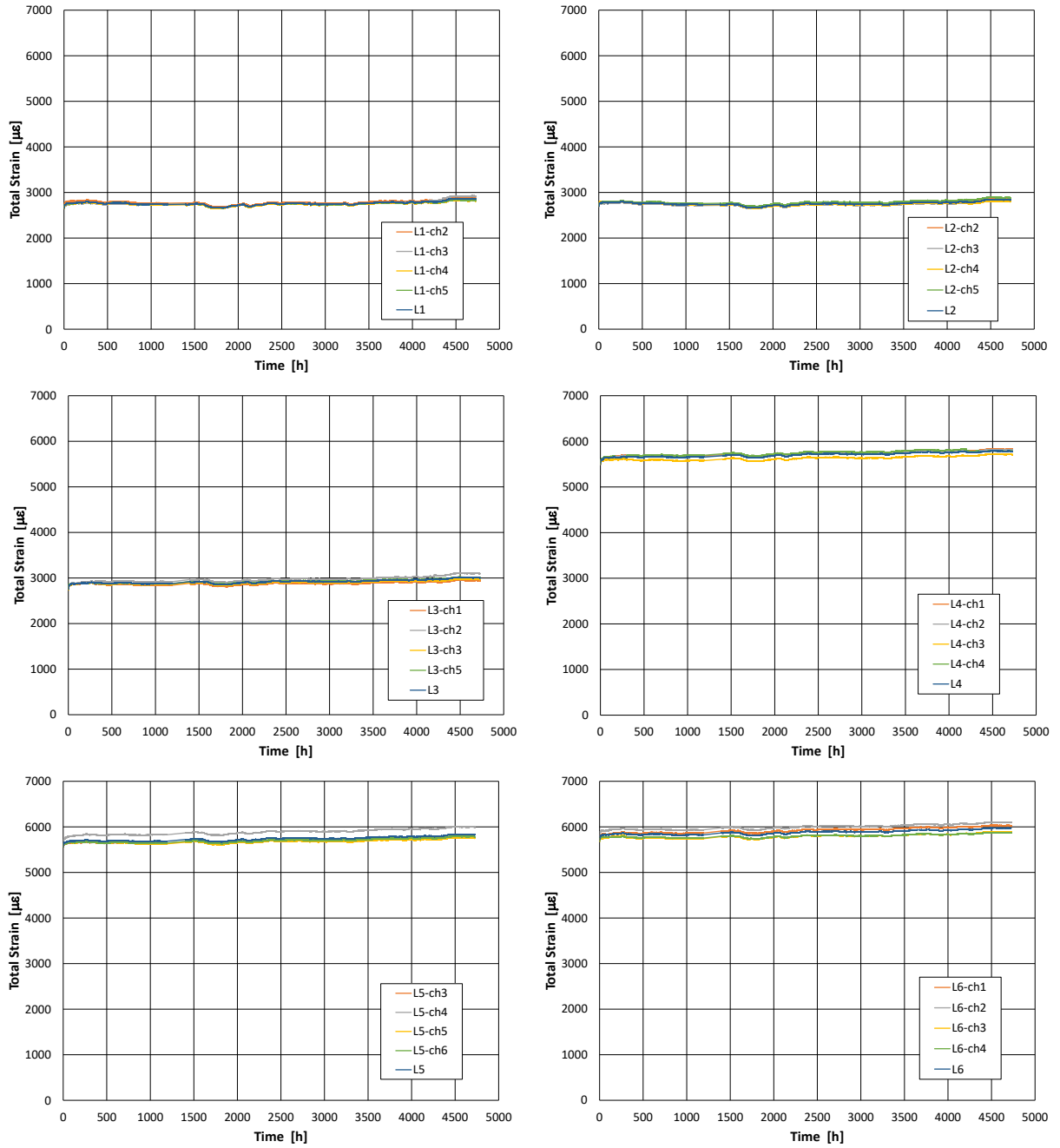


Figure 4. Deformations of the GFRP samples

The axial deformations of the fibre samples are highlighted in Figure 5 and have been obtained from the displacement measurements of specimen clamps edges by means of laser distance meters. Resulting strain variation over time is less than that recorded for laminates, although the viscous law is quite similar.

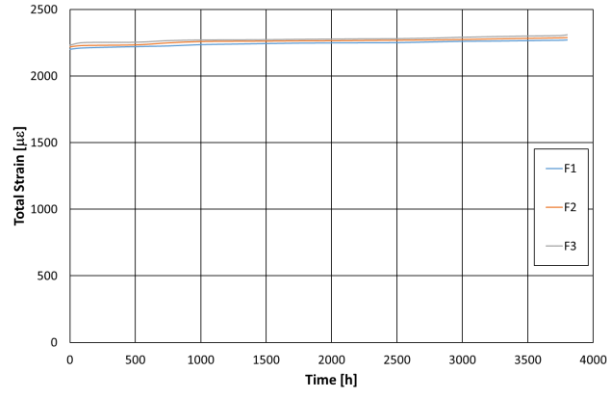


Figure 5. Deformations of the E-glass fibre samples

Total strain-time curves of the epoxy resin specimens are shown in Figure 6.

The diagrams of the M4 and M5 specimens are not presented, because they exhibited a sudden rupture at the beginning of creep test due to manufacturing defects.

The resin samples, unlike laminates and fibres, highlighted a significant primary creep stage followed by a high constant creep rate (secondary creep stage).

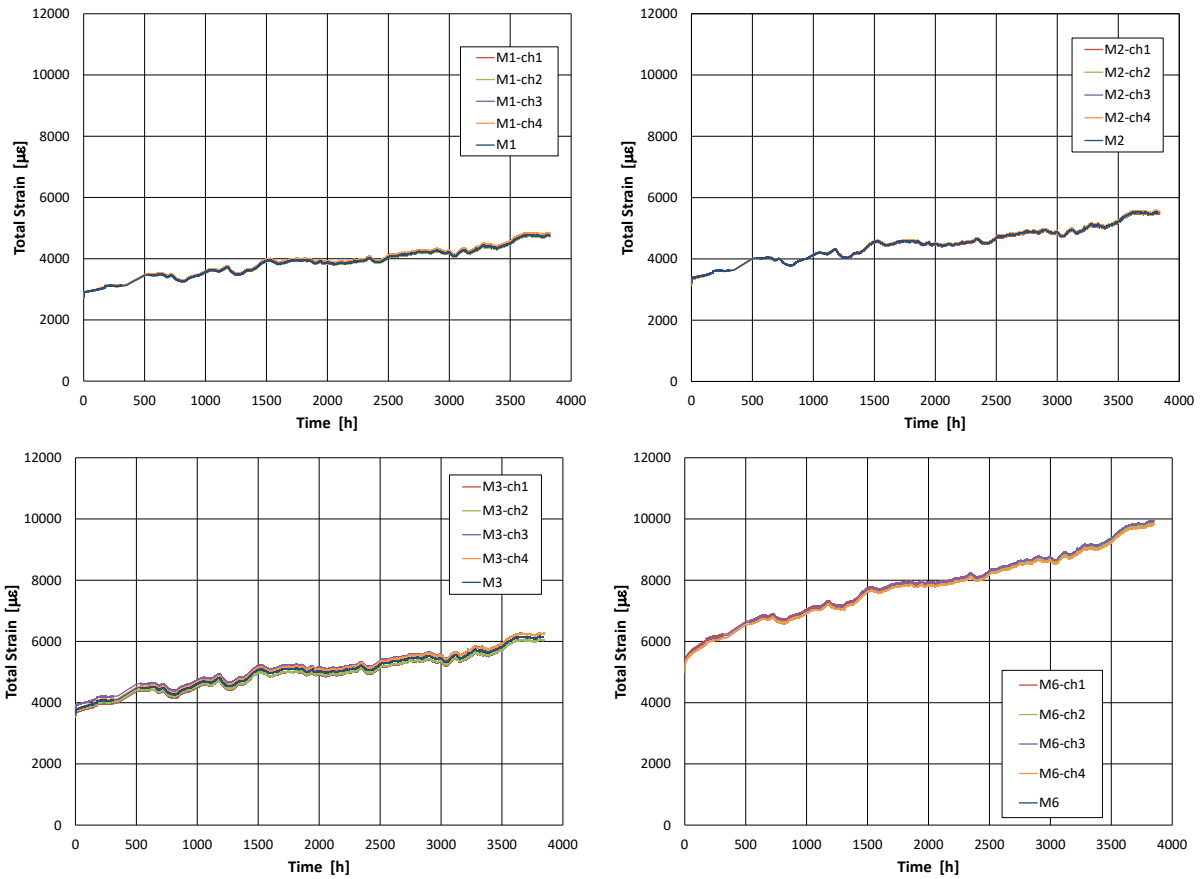


Figure 6. Deformations of the resins samples

The increase percentages of the axial deformations for the composites and their phases are reported in Tables 9, 10 and 11.

Table 9. Longitudinal deformations of the GFRP samples

Sample ID	$\varepsilon(t=0)$ [%]	$\varepsilon(t=100 h)$ [%]	$\varepsilon(t=1000 h)$ [%]	$\varepsilon(t=2500 h)$ [%]	$\varepsilon(t=4700 h)$ [%]	$\Delta\varepsilon/\varepsilon(t=0)$ [%]
L1	0.268	0.272	0.274	0.275	0.281	4.82
L2	0.270	0.276	0.277	0.278	0.284	4.88
L3	0.284	0.289	0.291	0.292	0.298	4.96
L4	0.551	0.560	0.565	0.573	0.577	4.74
L5	0.557	0.567	0.569	0.575	0.584	4.75
L6	0.573	0.582	0.582	0.590	0.599	4.57

Table 10. Longitudinal deformations of the E-glass fibre samples

Sample ID	$\varepsilon(t=0)$ [%]	$\varepsilon(t=100 h)$ [%]	$\varepsilon(t=1000 h)$ [%]	$\varepsilon(t=2500 h)$ [%]	$\varepsilon(t=3800 h)$ [%]	$\Delta\varepsilon/\varepsilon(t=0)$ [%]
F1	0.220	0.221	0.224	0.225	0.228	3.64
F2	0.222	0.223	0.226	0.227	0.231	4.05
F3	0.223	0.225	0.227	0.228	0.232	4.04

Table 11. Longitudinal deformations of the resin samples

Sample ID	$\varepsilon(t=0)$ [%]	$\varepsilon(t=100 h)$ [%]	$\varepsilon(t=1000 h)$ [%]	$\varepsilon(t=2500 h)$ [%]	$\varepsilon(t=3800 h)$ [%]	$\Delta\varepsilon/\varepsilon(t=0)$ [%]
M1	0.282	0.299	0.359	0.397	0.480	70.30
M2	0.323	0.346	0.415	0.460	0.552	70.92
M3	0.366	0.391	0.464	0.515	0.623	70.12
M6	0.507	0.576	0.699	0.815	0.996	96.52

The experimental results have highlighted a significant increase of the longitudinal strains in the epoxy resin samples over time, as well as limited deferred deformations in the laminates and fibre specimens. In particular, the difference between final strain and elastic strain $\Delta\varepsilon$ of resin specimens varies from 70% to about 100 %, whilst both laminates and fibres $\Delta\varepsilon$ is always less than 5%

It is worth noting that negligible primary creep has been shown by the fibres.

The creep compliance curves of GFRP laminates, fibres and epoxy resins are given in Figures 7, 8 and 9.

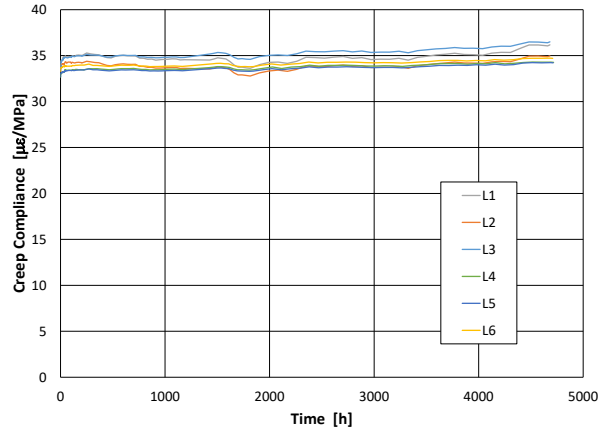


Figure 7. Creep compliance of the laminates

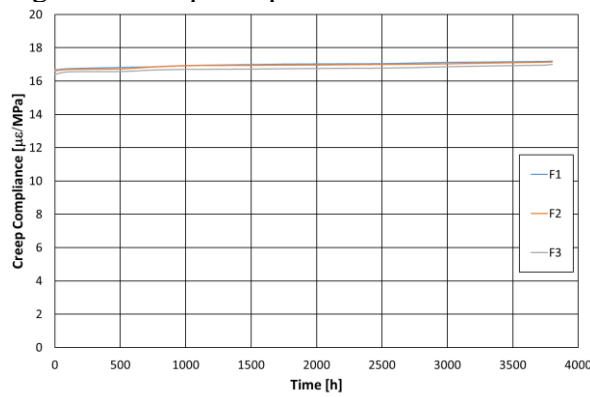


Figure 8. Creep compliance of the fibres

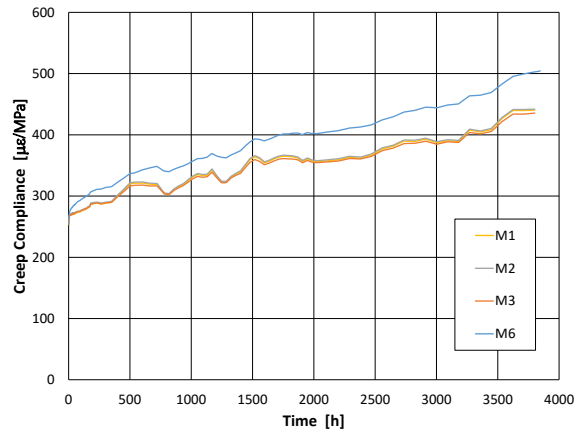


Figure 9. Creep compliance of the epoxy resins

The laminates and the fibres specimens have shown an almost perfect overlap of the creep compliance curves.

On the contrary, a different behavior occurred for the resin samples since the beginning of test (after about 10 h). Because of applied stress level, the specimen M6 is thus clearly dissimilar respect to M1, M2 and M3, highlighting a non linear viscous behavior.

4 PREDICTIVE VISCOUS MODELS

The long term behavior of the laminates and fibre samples has been characterized by means of Burger model, due to the linear viscoelastic behavior observed within the creep tests.

On the contrary, a non linear viscoelastic behavior has been recorded for the resins specimens and, then, their deferred behavior has been modelled through the non linear relationship proposed by the authors in [31].

4.1 VISCOUS MODELLING FOR THE LAMINATES AND FIBRE SAMPLES

The long term behavior of the laminates and the fibres has been modelled by using Burger rheological law (Figure 10), that allows for a good approximation of primary and secondary creep phenomena.

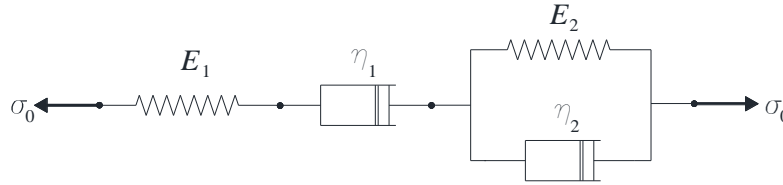


Figure 10. Burger viscous model.

More specifically, the creep response has been expressed by the relationship:

$$\varepsilon(t) = \sigma_0 \cdot \left[\left(\frac{1}{E_1} + \frac{t-t_0}{\eta_1} \right) + \frac{1}{E_1} \cdot \left(1 - e^{-\frac{(t-t_0) \cdot E_2}{\eta_2}} \right) \right] \quad (1)$$

Equation 1 has been rewritten as follows:

$$\varepsilon(t) = \sigma_0 \cdot \left[c_1 + c_2 \cdot (t-t_0) + c_3 \cdot \left(1 - e^{-\frac{(t-t_0) \cdot c_4}{c_3}} \right) \right], \quad (2)$$

where:

$$c_1 = \frac{1}{E_1}, \quad c_2 = \frac{1}{\eta_1}, \quad c_3 = \frac{1}{E_2}, \quad c_4 = \frac{1}{\eta_2}. \quad (3)$$

The creep compliance has been obtained from equation 2:

$$J(t, t_0) = \left[c_1 + c_2 \cdot (t-t_0) \right] + c_3 \cdot \left(1 - e^{-\frac{(t-t_0) \cdot c_4}{c_3}} \right). \quad (4)$$

The Burger coefficients for the laminates, $c_{i,FRP}$ ($i = 1, \dots, 4$), and the fibres, $c_{i,f}$, have been evaluated by fitting test data via the least-squares method [Tables 12, 13].

Table 12. Burger coefficients for the laminates

$C_{1,FRP}$ [MPa ⁻¹]	$C_{2,FRP}$ [MPa ⁻¹ h ⁻¹]	$C_{3,FRP}$ [MPa ⁻¹]	$C_{4,FRP}$ [MPa ⁻¹ h ⁻¹]
$3.3333 \cdot 10^{-5}$	$1.8391 \cdot 10^{-10}$	$5.3121 \cdot 10^{-7}$	$1.6575 \cdot 10^{-6}$

Table 13. Burger coefficients for the fibres

$C_{1,f}$ [MPa ⁻¹]	$C_{2,f}$ [MPa ⁻¹ h ⁻¹]	$C_{3,f}$ [MPa ⁻¹]	$C_{4,f}$ [MPa ⁻¹ h ⁻¹]
$1.6568 \cdot 10^{-5}$	$1.4388 \cdot 10^{-10}$	$1.0000 \cdot 10^{-50}$	$1.0000 \cdot 10^{-50}$

The predictive curves given by Burger model (B model) have been in good agreement with the experimental data (dots represent the experimental points), as shown in Figures 11 and 12.

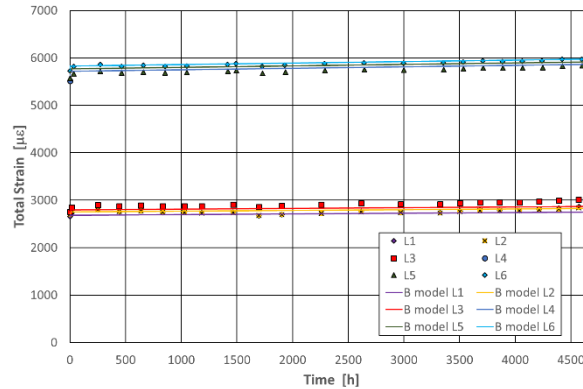


Figure 11. Predictive curves for the laminates specimens.

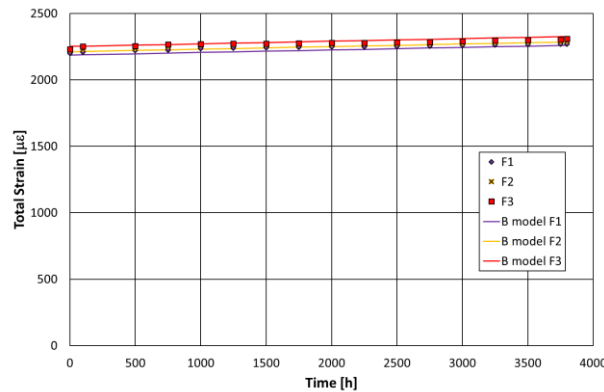


Figure 12. Predictive curves for the fibre specimens.

4.2 VISCOUS MODELLING FOR THE RESIN SAMPLES

The long term behavior of the resin specimens has been characterized by means of the nonlinear creep model proposed by the authors in [31]. Such a model (hereinafter named H&D model) was formulated accounting the primary, the secondary and the tertiary stages for variable stresses and temperature fields and it was implemented in the ANSYS FEM code.

Within the present study, no tertiary creep was observed and the creep test were performed at room temperature. Thus, the authors have restricted the general formulation of the H&D model to the primary and the secondary creep stages, by removing the tertiary (e.g. damage) one. The corresponding formulation has been expressed as follows:

$$\varepsilon_{cr} = \varepsilon_{cr}^I + \varepsilon_{cr}^{II} = \frac{1}{h_2 \cdot \sigma} \cdot \log\{1 + (1 + h_1) \cdot [\exp(h_2 \cdot c_1 \cdot \sigma^{c_2+1} \cdot t) - 1]\} \quad (5)$$

In the above formula, the parameters h_1 , h_2 , govern the primary creep stage, whereas c_1 , c_2 govern the secondary one.

The data fitting procedure has been achieved by splitting the primary and the secondary stages. Once the experimental points related to the secondary creep of the M_i curve have been selected, a linear fit of these data has been performed via the least-squares method into the (ε_{cr}, t) plane:

$$\varepsilon_{cr}(\sigma_i) = a_i \cdot t + b_i \quad (6)$$

where σ_i is the applied stress to the M_i specimen.

Let define the slant asymptote of the H&D creep model:

$$\varepsilon_{cr}(\sigma) = m \cdot t + q \quad (7)$$

The parameters m and q have been assumed, as function of σ , as follows:

$$m = c_1 \cdot \sigma^{c_2}; \quad q = d_1 \cdot \sigma^{d_2} \quad (8)$$

The constants c_1 , c_2 , have been obtained by fitting (a_i, σ_i) in logarithmic form via the least-squares method, whilst d_1 and d_2 have been fitted in logarithmic form via the least-squares method using (b_i, σ_i) .

On the other hand, the secondary stage has been characterized by the slant asymptote of the curve (7):

$$\lim_{t \rightarrow \infty} \left(\frac{\varepsilon_{cr}}{t} \right) = m = c_1 \cdot \sigma^{c_2} \quad (9)$$

Starting from the relationships (5) and (8), the following expression has been written:

$$\lim_{t \rightarrow \infty} (\varepsilon_{cr} - m \cdot t) = q = \frac{\log(1 + h_1)}{h_2 \sigma} = d_1 \cdot \sigma^{d_2} \quad (10)$$

Hence, the h_2 parameter is as follows:

$$h_2 = \frac{\log(1 + h_1)}{d_1 \cdot \sigma^{d_2-1}} \quad (11)$$

The h_1 parameter governs the primary stage and has been obtained via a non linear fit of all the creep data via the least-squares method.

The results of the proposed fitting procedure have been reported in Table 14.

Table 14. Material parameters for the H&D creep model, where stress is expressed in MPa, time in hours and temperature in K

Primary phase	Secondary phase			
h_1	c_1	c_2	d_1	d_2
31.20	4.11E-09	1.82	-11.90	1.6776

The predictive curves provided by the proposed H&D model have been in good agreement with the experimental results, as shown in Figures 13. An optimal fitting has been observed for the M6 specimen, because more experimental data points are involved in representing the primary creep stage of this sample.

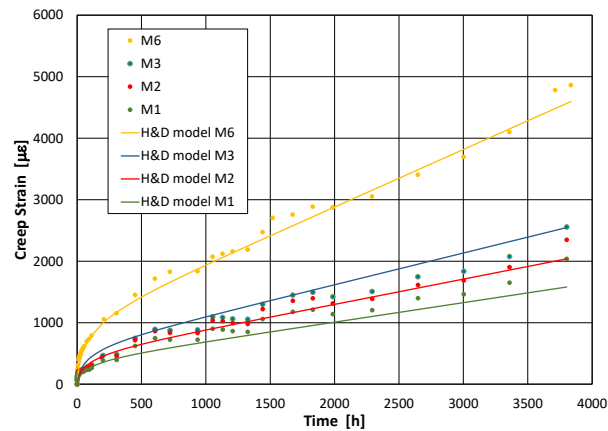


Figure 13. Predictive curves for the resin specimens

Experimental strain data of the M1, M2, M3 and M6 specimens at fixed instant times are plotted in Figure 14 and compared with the analytical H&D relationship.

It should be noted that with the increasing of time the non linearity in stress-creep strain curves becomes more evident, thus justifying an approach different from that proposed by the Burger model.

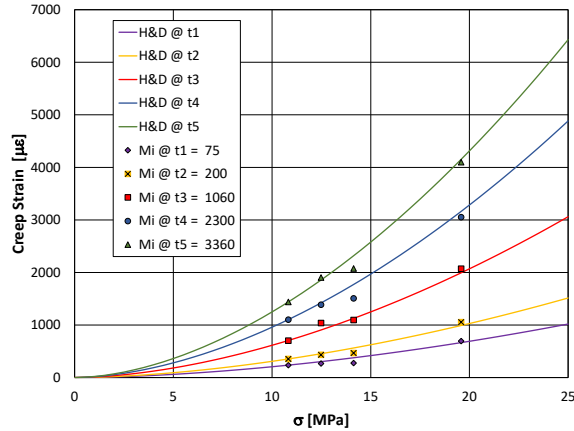


Figure 14. Stress-creep strain relationship with respect to different time levels

5. CONCLUDING REMARKS

In this paper, a theoretical and experimental investigation on creep phenomena of several unidirectional glass fibre reinforced polymer laminates, manufactured through the wet lay-up technique, and their constituent phases has been presented. The creep tests have been performed at different stress values at room temperature, by using steel devices designed by the authors.

The experimental data have highlighted significant deferred deformations in the epoxy resin samples over time from the early hours of observation. On the contrary, much less relevant viscous strains have been observed in the E-glass fibres and in the GFRP specimens.

The percentage strain increase of the resins after 3800 hours varies from 70% to about 100%, whilst the corresponding percentage variation of the laminates and fibres is less than 5%.

From a mechanical point of view, the GFRP laminates and the fibre samples have exhibited a linear viscoelastic behavior, while a non linear creep behavior has been observed for the resin specimens. Predictive viscous laws proposed for the tested composites and phases have been in good agreement with experimental data.

The outcomes of the creep tests on the GFRP laminates and E-glass fibres have shown a better rheological behavior than that expected in literature for mechanical, aeronautical and naval applications.

The results have pointed out the relevance of creep effects in epoxy resin and, thus, suggest performing long term verification of either composite members or existing structures strengthened with FRP, in order to evaluate the reliability and durability over time of such structural elements.

A further validation of the proposed model for the prediction of the non linear creep behavior of epoxy resin will be attempted based on the strains recording of the next six months.

ACKNOWLEDGEMENTS

The experimental investigation here presented has been developed within the activities of the research project funded by the Campania Region (Legge 5/2002).

REFERENCES

- [1] Ascione, L., Berardi, V.P., Anchorage device for FRP laminates in the strengthening of concrete structures close to beam-column joints (2011) *Composites Part B: Engineering*, 42 (7), pp. 1840-1850.
- [2] Ronagh, H.R., Eslami, A., Flexural retrofitting of RC buildings using GFRP/CFRP - A comparative study (2013) *Composites Part B: Engineering*, 46, pp. 188-196.
- [3] D'Ambrisi, A., Mezzi, M., Feo, L., Berardi, V.P., Analysis of masonry structures strengthened with polymeric net reinforced cementitious matrix materials (2014) *Composite Structures*, 113 (1), pp. 264-271.
- [4] Fabbrocino, F., Farina, I., Berardi, V.P., Ferreira, A.J.M., Fraternali, F., On the thrust surface of unreinforced and FRP-/FRCM-reinforced masonry domes (2015) *Composites Part B: Engineering*, 83, pp. 297-305.
- [5] Cricri, G., Perrella, M., Investigation of mode III fracture behaviour in bonded pultruded GFRP composite joints, (2017) *Composites Part B: Engineering*, 112, pp. 176-184. DOI: 10.1016/j.compositesb.2016.12.052
- [6] Cricri, G., Perrella, M., Sessa, S., Valoroso, N., A novel fixture for measuring mode III toughness of bonded assemblies (2015) *Engineering Fracture Mechanics*, 138, pp. 1-18.
- [7] Citarella, R., Cricri, G., Three-dimensional BEM and FEM submodelling in a cracked FML full scale aeronautic panel (2014) *Applied Composite Materials*, 21 (3), pp. 557-577.
- [8] Corato V., Affinito L., Anemona A., Besi Vetrella U., della Corte A., Di Zenobio A., Fiamozzi Zignani C., Freda R., Messina G., Muzzi L., Perrella M., Reccia L., Tomassetti G., Turtù S., Detailed design of the large-bore 8T superconducting magnet for the NAFASSY test facility (2015) *Superconductor Science and Technology*, 28(3), art. no. 034005.
- [9] Alwis, K. G. N. C., Burgoyne, C. J., Time-Temperature Superposition to Determine the Stress-Rupture of Aramid Fibres, *Applied Composite Materials*, 13(4), (2006).
- [10] Burgoyne, C. J., Alwis, K. G. N. C., Visco-elasticity of aramid fibres, *Journal of Materials Science*, 43(22), (2008).
- [11] Ascione, F., Berardi, V.P., Feo, L., Giordano, A., An experimental study on the long-term behavior of CFRP pultruded laminates suitable to concrete structures rehabilitation (2008) *Composites Part B: Engineering*, 39 (7-8), pp. 1147-1150.
- [12] Ascione, L., Berardi, V.P., D'Aponte, A., Creep phenomena in FRP materials (2012) *Mechanics Research Communications*, 43, pp. 15-21.
- [13] Karim Benzarti, Nourredine Houhou, Marc Quiertant, Sylvain Chataigner. Creep behavior of cold-curing epoxy adhesives: analysis and predictive approach (2014) *Composites In Civil Engineering (CICE)*, Aug 2014, VANCOUVER, Canada.
- [14] N. Houhou, K. Benzarti, M. Quiertant, S. Chataigner, A. Fléty, and C. Marty, Analysis of the nonlinear creep behavior of concrete/FRP-bonded assemblies (2014) *Journal of Adhesion Science and Technology* Vol. 28 , Iss. 14-15.
- [15] Shi, J., Wang, X., Wu, Z., Zhu, Z., Creep behavior enhancement of a basalt fiber-reinforced polymer tendon(2015) *Construction and Building Materials*, 94, art. no. 6933, pp. 750-757.
- [16] Zhang, X., Huang, Q., Chen, J., Li, Z., Prediction of viscoelastic behavior of unidirectional polymer matrix composites (2016) *Journal Wuhan University of Technology, Materials Science Edition*, 31 (3), pp. 695-699.
- [17] Georgiopoulos, P., Kontou, E., Christopoulos, A., Short-term creep behavior of a biodegradable polymer reinforced with wood-fibers (2015) *Composites Part B: Engineering*, 80, pp. 134-144.

- [18] Daghigh, V., Khalili, S.M.R., Eslami Farsani, R., Creep behavior of basalt fiber-metal laminate composites (2016) *Composites Part B: Engineering*, 91, pp. 275-282.
- [19] Rwawiire, S., Tomkova, B., Wiener, J., Militky, J., Kasedde, A., Kale, B.M., Jabbar, A., Short-term creep of barkcloth reinforced laminar epoxy composites (2016) *Composites Part B: Engineering*, 103, pp. 131-138.
- [20] Nedjar, B., Modeling long-term creep rupture by debonding in unidirectional fibre-reinforced composites (2014) *International Journal of Solids and Structures*, 51 (10), pp. 1962-1969.
- [21] Berardi, V.P., Mancusi, G., Time-dependent behavior of reinforced polymer concrete columns under eccentric axial loading (2012) *Materials*, 5 (11), pp. 2342-235.
- [22] Jiang, W., Gong, J., De Schutter, G., Huang, Y., Yuan, Y., Time-dependent analysis during construction of concrete tube for tower high-rise building (2012) *Structural Concrete*, 13 (4), pp. 236-247.
- [23] Berardi, V.P., Mancusi, G., A mechanical model for predicting the long term behavior of reinforced polymer concretes (2013) *Mechanics Research Communications*, 50, pp. 1-7.
- [24] Wu, D., Gao, W., Feng, J., Luo, K., Structural behaviour evolution of composite steel-concrete curved structure with uncertain creep and shrinkage effects (2016) *Composites Part B: Engineering*, 86, pp. 261-272.
- [25] Sá, M.F., Gomes, A.M., Correia, J.R., Silvestre, N., Flexural creep response of pultruded GFRP deck panels: Proposal for obtaining full-section viscoelastic moduli and creep coefficients (2016) *Composites Part B: Engineering*, 98(1), pp 213-224.
- [26] Nedjar, B., Directional damage gradient modeling of fiber/matrix debonding in viscoelastic UD composites (2016) *Composite Structures*, 153, pp. 895-901.
- [27] Ascione, L., Berardi, V.P., D'Aponte, A., A viscoelastic constitutive law for FRP materials (2011) *International Journal of Computational Methods in Engineering Science and Mechanics*, 12 (5), pp. 225-232.
- [28] Mancusi, G., Spadea, S., Berardi, V.P., Experimental analysis on the time-dependent bonding of FRP laminates under sustained loads (2013) *Composites Part B: Engineering*, 46, pp. 116-122.
- [29] Ascione, L., Berardi, V.P., D'Aponte, A., Long-term behavior of PC beams externally plated with prestressed FRP systems: A mechanical model (2011) *Composites Part B: Engineering*, 42 (5), pp. 1196-1201.
- [30] Lou, T., Lopes, S.M.R., Lopes, A.V., Time-dependent behavior of concrete beams prestressed with bonded AFRP tendons (2016) *Composites Part B: Engineering*, 97, pp.1-8.
- [31] C. Cali, G. Cricri, M. Perrella, An Advanced Creep Model for Hardening and Damage Effects (2010), *Strain*, 46, pp. 347–357.